

Kinetic shift in chlorobenzene ion fragmentation and the heat of formation of the phenyl ion

Henry M. Rosenstock and Roger Stockbauer

National Bureau of Standards, National Measurement Laboratory, Washington, D.C. 20234

Albert C. Parr^{a)}

Department of Physics and Astronomy, University of Alabama, University, Alabama 35486

(Received 25 June 1979; accepted 20 July 1979)

The fragmentation of chlorobenzene ion has been studied by photoelectron-photoion coincidence techniques. By varying the residence time it is possible to obtain breakdown curves as a function of residence time. The parent-daughter transition region shifts to lower energies as the residence time is increased (kinetic shift). The shift is of the order of 0.4 eV in going from 0.7 to 8.9 μs . A systematic analysis of the breakdown curves and residence time effects has been carried out using quasiequilibrium theory. The experimental results and analysis lead to $\Delta H_{f_0}^\circ$ (phenyl ion) = 275 ± 1 kcal/mol (1151 ± 4 kJ/mol). The systematic analysis shows that this experiment leads to a quite accurate rate-energy curve in the range of 10^4 – 10^6 s⁻¹. The sensitivity of the QET model has been studied, and the limitations to the determination of activated complex parameters is critically discussed. The parameters obtained in this work are rather similar to those of an analogous neutral process, i.e., thermal decomposition of bromobenzene.

I. INTRODUCTION

The existence of a kinetic shift in ion fragmentation threshold measurements was pointed out many years ago.^{1,2} More recently a number of experimental approaches of increasing sophistication have been used to study this effect.^{3–10} The problem of deducing a “threshold” from an ion yield vs energy experiment is of course equivalent to deducing the activation energy of the ion fragmentation process.

A different class of experiments, photoelectron-photoion coincidence experiments^{11–15} and charge exchange experiments^{16,17} in which the energy content of the ion can be more sharply defined and varied in a controlled manner provides more direct experimental information on the rate-energy dependence from which the activation energy and entropy may be deduced. It must be noted, however, that this rate-energy information can only be effectively extracted after careful definition of the apparatus function and appropriate folding or unfolding of the available and desired information. Further, it is necessary to take into account the thermal vibrational and rotational energy distribution of the molecule.^{18,19} The effect of these distributions is to produce a distribution of unimolecular decomposition rates. This distribution produces some smearing out in all experiments where the energy input is otherwise sharply defined.

The purpose of the present study is to apply the recently developed technique¹⁰ of photoelectron-photoion coincidence mass spectrometry with variable residence time to a study of the positive ion fragmentation of chlorobenzene, forming the phenyl ion and a chlorine atom. The process is one which is expected to exhibit a significant kinetic shift and, in contrast to allene fragmentation studied previously,¹⁰ should represent a truly simple

bond breaking process. Analysis of the time dependent parent-daughter breakdown curves in a manner analogous to the allene analysis should yield accurate kinetic parameters for the unimolecular decomposition and an accurate $\Delta H_{f_0}^\circ$ for the phenyl ion. In addition the results afford an interesting comparison with an earlier study of this molecule by Baer and co-workers,²⁰ using a somewhat different electron-ion coincidence apparatus and different mode of data analysis appropriate to their experiment. Bouchoux²¹ carefully analyzed the time dependence of the electron impact appearance potential and was able to deduce a kinetic shift and an activation energy for the same process.

II. EXPERIMENTAL

The kinetic shift data were obtained with the threshold photoelectron-photoion coincidence mass spectrometer described previously.²² The method uses monochromatized photons to photoionize a gaseous sample. The electrons from the reaction $\text{C}_6\text{H}_5\text{Cl} + h\nu \rightarrow \text{C}_6\text{H}_5^+ + \text{Cl} + e$ are filtered so only those having zero initial kinetic energy (threshold photoelectrons) are detected. This insures that the parent ions have a known excitation energy imparted in the ionization process. The ion from the reaction is time-of-flight (TOF) mass analyzed and detected in coincidence with the threshold photoelectron. The TOF mass analyzer operates in the pulsed mode, using the detection of a threshold photoelectron as the trigger. This drawout pulse can be externally delayed so that the time between the production of the ion and its detection can be varied.¹⁰ Since this time is known precisely and is variable in the experiments, the kinetic shift, i.e., the change in the breakdown curve as a function of fragmentation time can be determined accurately.

Two TOF coincidence mass spectra are shown in Fig. 1. Both were obtained at the same photon energy but with different drawout pulse delay times, 0.7 and 5.7 μs , respectively. As expected, at the longer ion

^{a)} Intergovernmental Personnel Act Appointee at the National Bureau of Standards, 1978–1979.

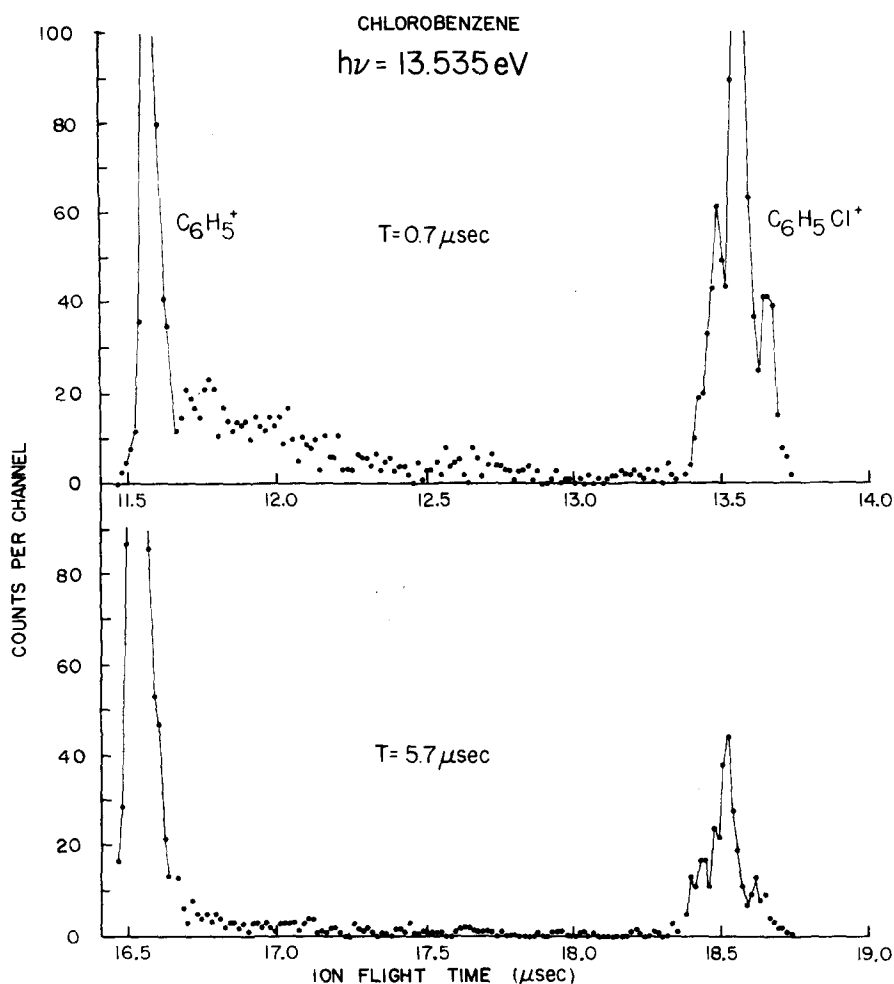


FIG. 1. Coincidence time of flight spectra experimentally observed for 0.7 and 5.7 μs effective ion residence time.

residence time, the parent ion intensity (right-hand peak) has decreased while the fragment ion intensity (left-hand peak) has increased.

Also there are a large number of ion counts distributed throughout the TOF region between the two peaks. These are metastable ions, i. e., those ions which fragment in the acceleration region. They are more prominent in the upper of the two spectra shown in Fig. 1.

Due to the large metastable ion contribution; the extraction of the breakdown curve from this data is not as straightforward as in our previous work¹⁰ where the metastable ion intensity was negligible. Neglect of the metastable ions in the present case would introduce some error in the parent-daughter ratios required for construction of the experimental breakdown curve. However, the large metastable ion intensity allows us to extract two sets of breakdown curves from each drawout pulse delay setting as discussed below.

The metastable ions are those ions which fragment after the drawout pulse is applied but before they reach the end of the acceleration region. Hence, by adding the metastable ion intensity to the parent peak, we obtain the amount of fragmentation occurring before the drawout pulse is applied. Alternatively, by adding the metastable intensity to the fragment peak we obtain the amount of fragmentation occurring before the parent ions

reach the end of the acceleration period.

This treatment of the TOF spectra gives us two independent breakdown curves whose effective ion residence time differs by the time the ions spend in traversing the acceleration region. The TOF spectra were taken at two delay times so a total of four breakdown curves were obtained.

The residence time for the first set of breakdown curves is the time between the formation of the electron-ion pair and the application of the in drawout pulse. This is the sum of the electron flight time which is calculated from the acceleration potentials and distances and the drawout pulse delay time which is measured. It is known to within ± 50 ns, the uncertainty arising primarily from uncertainty in the electron flight time. The resulting breakdown curves obtained with 0.7 and 5.7 μs residence times are displayed in Fig. 2 along with the calculated "best fit" breakdown curves.

The effective residence time for the second set of breakdown curves is obtained by adding the parent ion acceleration time to the residence time defined above. Thus the total fragmentation time is the sum of the electron flight time, drawout pulse delay time, and parent ion acceleration time. This ion acceleration time is calculated from the fields and distances used in the TOF analyzer. It is calculated to be $3.2 \pm 0.2 \mu\text{s}$ where again

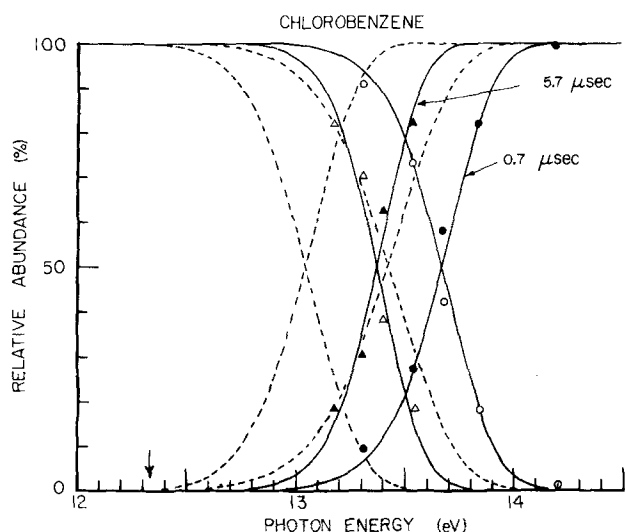


FIG. 2. Breakdown curves for chlorobenzene for 0.7 and 5.7 μs effective residence times. Experimental points: (O), (Δ) $\text{C}_6\text{H}_5\text{Cl}^+$ parent; (\bullet), (\blacktriangle) C_6H_5^+ fragment; (—) best fit calculations; (---) calculations using parameters of Baer *et al.*²⁰ Arrow indicates thermochemical threshold.

the uncertainty is due to uncertainty in the true potentials and distances involved. The second set of breakdown curves for 3.9 and 8.9 μs effective residence time (3.2 μs added to the previous 0.7 and 5.7 μs times) are shown in Fig. 3 along with calculated best fit breakdown curves. This data is not as precise as the shorter time data due to the relatively large uncertainty in the calculated ion flight time.

III. ANALYSIS OF THE DATA

The data were analyzed in the same general manner as was done for allene.¹⁰ Briefly, a rate-energy curve (actually a table at 0.005 eV intervals) was calculated using a set of reactant ion and activated complex frequencies and an assumed activation energy. The rates were calculated using the full Laplace transform method²³⁻²⁵ and numerical inversion of the Laplace transform to give the reactant and activated complex density of states. A fragmentation time was then chosen and a breakdown curve calculated. The breakdown curve was then convoluted with the ion energy sampling function of the apparatus, i. e., the mirror image of the electron energy analyzer transmission function. This experimentally determined apparatus function also contains a contribution from the finite resolution of the photon monochromator. Following this, two more convolutions were carried out to allow for a room-temperature three-dimensional classical rotor energy distribution and the room temperature vibrational population for the chlorobenzene molecule. The apparatus and rotor functions are identical to those shown in the allene study¹⁰ and the vibrational population distribution was only slightly broader than that shown for allene.

For our initial calculations the reactant ion frequencies were assumed to be the same as those of the neutral chlorobenzene molecule as determined by Whiffen.²⁶ The activated complex frequencies were chosen by sim-

ply reducing all the frequencies (except the one transformed into the reaction coordinate) by a fixed percentage following the earlier work of Baer *et al.*²⁰

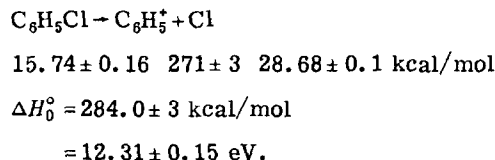
The initial value of the activation energy (which was subsequently iterated) was determined as follows:

Rodgers, Golden, and Benson²⁷ have studied the kinetics of the reaction of iodobenzene and hydrogen iodide. From their results they conclude that $\Delta H_{f_{298}}^\circ(\text{C}_6\text{H}_5, g) = 80.0 \pm 1$ kcal/mol and $\Delta H_{298}^\circ(\text{C}_6\text{H}_5\text{-H}) = 112.3$ kcal/mol. Thus we have for the process C_6H_6 (benzene) $\rightarrow \text{C}_6\text{H}_5$ (phenyl) + H $\Delta H_{298}^\circ = 112.3 \pm 1$ kcal/mol.

This datum can be reduced to absolute zero by standard translational, rotational, and vibrational heat capacity arguments. With the assumption that the vibrational heat capacity function of phenyl radical is the same as that of benzene (the missing CH stretch and two bends make no significant contribution below room temperature) one obtains $\Delta H_{f_0}^\circ(\text{C}_6\text{H}_5) = 84.2 \pm 1$ kcal/mol. Using the Sergeev *et al.*²⁸ measurement of the phenyl radical ionization potential, 8.1 ± 0.1 eV, we obtain $\Delta H_{f_0}^\circ(\text{C}_6\text{H}_5^+) = 271 \pm 3$ kcal/mol.

The remaining quantity needed for calculation of ΔH_0 is $\Delta H_{f_0}^\circ(\text{C}_6\text{H}_5\text{Cl})$. This is determined from $\Delta H_{f_{298}}^\circ(\text{C}_6\text{H}_5\text{Cl}) = 12.26 \pm 0.16$ kcal/mole.²⁹ The heat capacity correction was made using the vibrational frequencies given by Whiffen,²⁶ along with other tabulated values,³⁰ giving $\Delta H_{f_0}^\circ(\text{C}_6\text{H}_5\text{Cl}) = 15.74 \pm 0.16$ kcal/mol.

Finally we have for the process



And using I. P. ($\text{C}_6\text{H}_5\text{Cl}$) = 9.07 ± 0.02 eV²⁰ we have a ΔH_0 for the reaction of 3.24 ± 0.16 eV which we equate to the activation energy of the process.

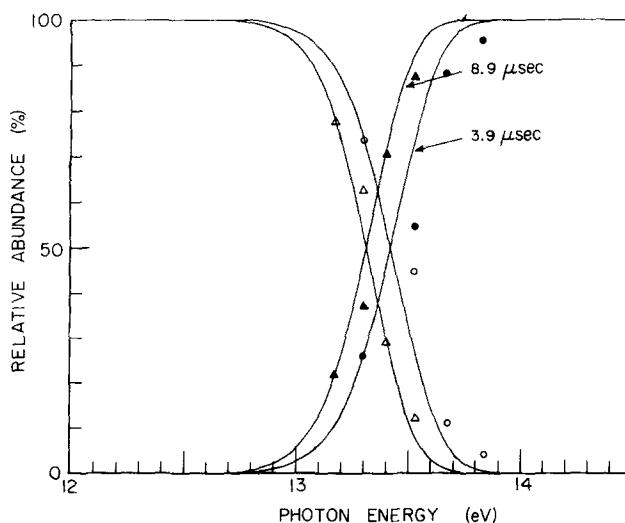


FIG. 3. Breakdown curves for chlorobenzene for 3.9 and 8.9 μs effective ion residence time. Experimental points: (O) (Δ) $\text{C}_6\text{H}_5\text{Cl}^+$ parent; (\bullet), (\blacktriangle) C_6H_5^+ fragment; (—) best fit calculations.

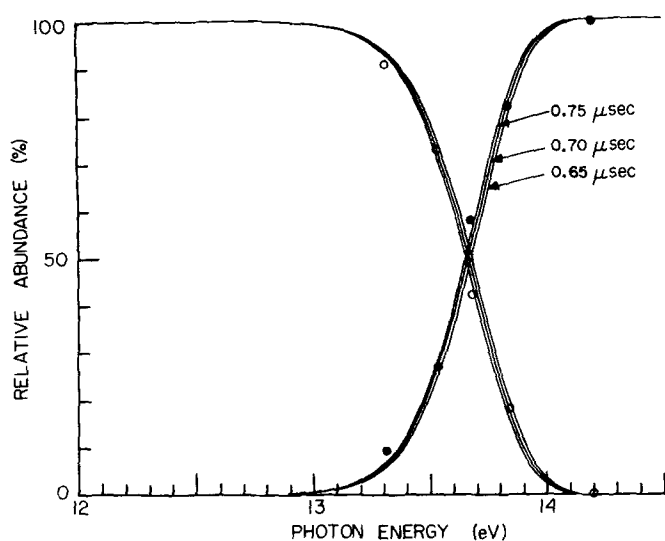


FIG. 4. (—) Calculated breakdown curves showing sensitivity to ion residence time. Experimental points: (○) $C_6H_5Cl^+$ parent, (●) $C_6H_5^+$ fragment.

IV. RESULTS

In Fig. 2 are shown the best fit breakdown curves (solid lines) calculated at 0.7 and 5.7 μs residence time along with the experimental points. The activated complex parameters were an activation energy of 3.26 eV and a frequency reduction of 23% in all activated complex modes. The fit is very good. Also shown is the thermochemical 0 K threshold indicated by a vertical arrow. Clearly there is a large kinetic shift, of the order of (0.7–1.1 eV) depending on the residence time. Also as shown in Fig. 3, for the somewhat less precise experimental data for 3.9 and 8.9 μs residence times, the calculations (solid lines) and experiments are in reasonably good agreement except for one pair of points.

V. DISCUSSION

The activation energy of 3.26 eV deduced from our experimental results is in rather good agreement with the ΔH_0 of 3.24 ± 0.15 eV which was calculated above from independent thermochemical information. Nevertheless, a number of points must be more closely scrutinized: the sensitivity of the calculations, the meaningfulness of the activated complex models and parameters, and comparison of our results with the earlier results obtained by Baer *et al.*²⁰ Also a comparison of the kinetic parameters deduced here with those for the analogous thermal decomposition reaction of neutral bromobenzene is instructive. Unfortunately, data on chlorobenzene are unavailable.

A. Sensitivity analysis

As mentioned above, the time delay in the drawout pulse is known only to ± 50 ns. This uncertainty will have the greatest effect on the breakdown curves calculated for the shortest residence time, i. e., 0.7 μs . To observe what effect the 50 ns uncertainty had on the curves, calculations were carried out for 0.65 and 0.75 μs as well. The comparison with the experimental

points is shown in Fig. 4. As expected, there is some shift in the calculated breakdown curves. We take these results as indicating that the given choice of activated complex parameters fit the experimental results to within the accuracy of our knowledge of the delay time. The calculated breakdown curves for the longer residence times are even less sensitive to this uncertainty.

In carrying out these rate calculations we adopted an activated complex model similar to that adopted by Baer *et al.*²⁰ The looseness of the activated complex was represented by lowering the frequencies of *all* the normal modes by a given percentage. One can test the sensitivity of the results to the assumed activation energy and extent of frequency lowering by constructing a so-called crossover sensitivity plot.¹⁰ For the two most accurate sets of data points, 0.7 and 5.7 μs fragmentation time we can determine the point on the photon energy scale at which 50% fragmentation occurs. This defines a crossover energy for 5.7 μs and a crossover shift, i. e., the additional energy necessary to achieve 50% fragmentation in the shorter 0.7 μs fragmentation time. As expected, a larger activation energy produces a larger crossover energy and a larger crossover shift since the rate-energy dependence is less steep for larger activation energy. On the other hand, a looser activated complex (more positive entropy of activation) will have just the opposite effect. So, the two experimental observables, crossover energy and crossover shift, can be tested against two calculational parameters, activation energy and activation entropy.

The entropy of activation is calculated for a hypothetical thermal unimolecular decomposition, using standard methods of statistical thermodynamics, at an arbitrarily chosen temperature of 1000 K (see further discussion below). The change in crossover energy and crossover shift for different activation energies and activation entropies is shown in Fig. 5. The figure clearly exhibits the energy-entropy tradeoff discussed above. Also shown is the crossover energy and cross-

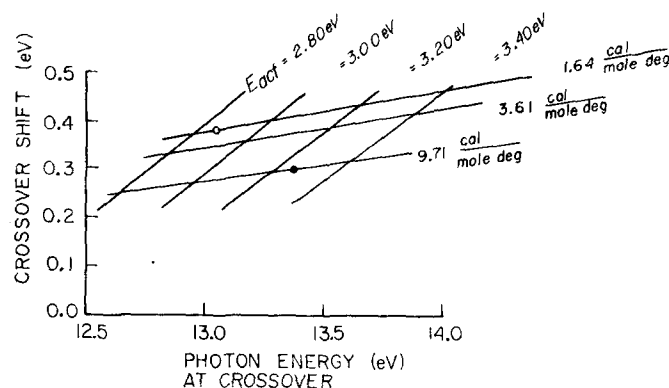


FIG. 5. Sensitivity of the calculated chlorobenzene breakdown curves to activation energy, E_{act} , and activation entropy. The curves show the change in the crossover energy (energy at the 50% point in the long time parent-fragment curves) and the change in the crossover shift (energy difference between the crossover points of the breakdown curves obtained at two different times). (●) Crossover energy and shift obtained from Fig. 2. (○) Activated complex parameters used by Baer *et al.*²⁰

TABLE I. Kinetic parameters determined from crossover sensitivity analysis.

Model	E_{act} , eV	ΔS_{1000}^\ddagger , eu	A_{1000} , s^{-1}	$A_{classical}$
I	3.26 ± 0.02	9.71 ± 0.4	6.62×10^{14}	4.12×10^{16}
II	3.37 ± 0.02	9.90 ± 0.4	1.31×10^{15}	7.82×10^{15}
III	3.43 ± 0.02	10.00 ± 0.4	1.92×10^{15}	6.00×10^{15}

over shift determined from our experiment (black point). Our results indicate that for this model the activation energy is 3.26 ± 0.2 eV and the equivalent 1000 K entropy is 9.71 ± 0.4 eu.

B. The activated complex model

The model used in the present calculations to this point allows for looseness by lowering all activated complex frequencies by some percentage. The spectroscopic analysis of Whiffen²⁶ shows that of the thirty normal modes of chlorobenzene only six involve the force constants of the carbon-halogen bond. Thus, the activated complex parameters adopted so far (Model I) are not particularly plausible.

In order to investigate this, two additional models were studied. In one (Model II) only the five halogen sensitive modes (1085, 416, 297, 467, 196 cm^{-1}) other than the one becoming the reaction coordinate (702 cm^{-1}) were set equal and numerical values of this set of equal frequencies were varied. In the other (Model III) model only the two modes corresponding most closely to in-plane and out-of-plane halogen bending (297 and 196 cm^{-1}) were decreased by varying percentages. Following the crossover sensitivity analysis outlined above it was possible to establish kinetic parameters which fit the crossover energy and shift. The results for all three models are compared in Table I. These results reveal some of the limitations which are encountered in the analysis of this type of information, and there are close parallels to the limitations encountered in thermal unimolecular kinetics.

Digressing for a moment to thermal kinetics, it is evident that from one rate at one temperature one cannot deduce separately an energy and an entropy of activation. Information on rates over a range of temperature permits one to determine an experimental activation energy and entropy via an Arrhenius plot, and many sets of activated complex properties can account for the experimental activation entropy. Rate information over an extremely wide temperature range begins to reveal curvature in Arrhenius plots,³¹ permitting one to detect the temperature dependence of the activation entropy and, consequently, imposing some limitations on the choice of activated complex properties.

In the present experiments we gain implicit information about decomposition rate constants in a range of values dictated by the range of decomposition time and apparatus sensitivity. This range is roughly 1×10^4 – 3×10^6 s^{-1} , corresponding to roughly 10% fragmentation at 8.9 μs and 90% fragmentation at 0.7 μs . It is instructive to compare the rate-energy dependence for

this range as calculated from the three sets of best fit activated complex parameters. The results are shown in Fig. 6 for Model I (solid line) Model II (○), and Model III (●). The three curves are extremely close but not totally identical (as indeed they cannot be). Thus the experiment leads in this instance to a quite reliable specification of the rate-energy dependence for a broad range of activated complex models. In effect, the experiment can only be accounted for by a small range of rate energy curves in this time interval ($\sim 10^{-4}$ – 10^{-7} s). In passing, it should be mentioned that although we worked only with the crossover energy and shift to specify the parameters, the entire calculated breakdown curves for all three models fit all data points as well as was shown for Model I in Fig. 2.

If we now proceed to the limit of high energy—the classical limit—the rate approaches

$$k = \frac{1}{h} \frac{\prod_i \nu_i}{\prod_j \nu_j^\ddagger} \left(\frac{E - E_{act}}{E} \right)^{s-1}$$

and the limiting rate is just the ratio of the product of the frequencies. The three models give limiting rates which differ by a factor of seven, shown in Table I under $A_{classical}$. This, of course reflects the limitation of the accessible range of rates on the specification of the activated complex parameters.

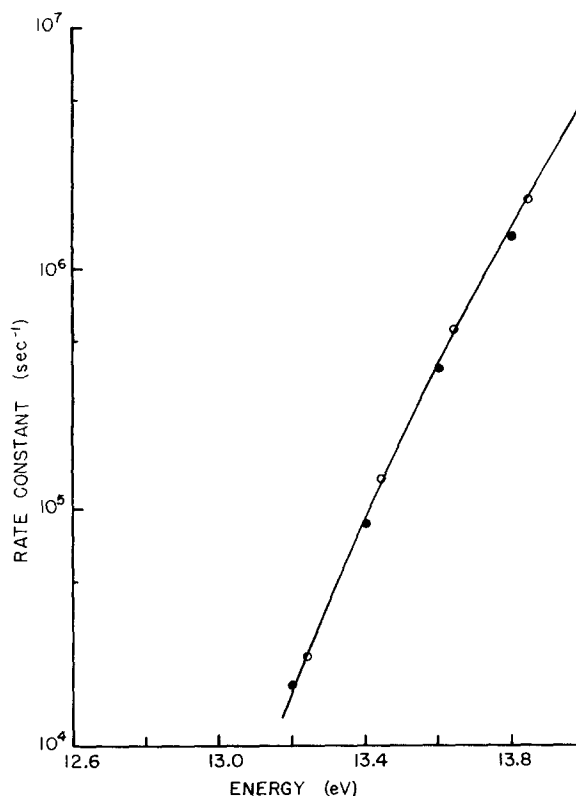


FIG. 6. Rate energy curves calculated for the three models discussed in the text. The activated complex parameters are those which reproduce the data in Fig. 2 and are summarized for each model in Table I. (—) Model I, (○) Model II, (●) Model III.

At the reaction threshold, the rate is given by $1/h\rho(E_{act})$, and it is seen, again from Table I, that the threshold rate is different for the three models because the activation energies differ. The model with the highest classical limit has the lowest threshold rate.

On the basis of this discussion we conclude that the most likely value of the activation energy is 3.40 ± 0.05 eV and the equivalent 1000 K activation entropy is 9.995 ± 0.4 eu. (The activated complex implied by Model I is too implausible). This energy may be compared to the thermochemical value 3.24 ± 0.15 eV discussed earlier. Our results lead to $\Delta H_{f_0}^\circ(C_6H_5^+) = 275 \pm 1$ kcal/mol.

This value may be compared to the ion heat of formation determined by Beauchamp³² from the phenyl fluoride heterolytic bond dissociation energy. They reported a value of 270 ± 4 kcal/mol. This value refers presumably to an ICR equilibrium measurement at or near room temperature. Assuming the $C_6H_5^+$ heat capacity is the same as C_6H_5 and C_6H_6 the value should be about 4 kcal/mol higher than the zero Kelvin value. The other reported value⁶ is based on a carefully calibrated non-monoenergetic appearance potential measurement on benzene. The apparatus was modified to provide long residence times in the ion source ($> 10^{-4}$ s) to overcome kinetic shift. The measured appearance potential is several tenths of an eV below the thermochemical threshold for



computed from $\Delta H_{f_0}^\circ(C_6H_5^+) = 275$ kcal/mol. Part of the deviation is due to the nonnegligible population of vibrationally excited benzene molecules. At room temperature, the population extends out significantly past 0.1 eV⁹ and at the ion source temperature of the apparatus it may well extend further.

C. Comparison with the results of Baer *et al.*²⁰ and Bouchoux²¹

Several years ago Baer and co-workers studied the same fragmentation process in their coincidence apparatus.²⁰ They determined time of flight distributions of the parent-metastable-daughter ions at different excitation energies. The excitation energies were determined by the photon energy and by restriction to events in coincidence with photoelectrons near zero energy, in a manner very similar to the present experiment. For each energy the entire time of flight distribution was fit by a single ion lifetime and suitably folded into their apparatus function. From this they determined a set of rate constants at different energies and fit their rate-energy data to a calculated rate-energy curve. For activated complex parameters they used an activation energy of 2.86 eV and adjusted all activated complex frequencies (the same frequency adjustment as was used in our Model I calculation). With that activation energy, they found that an 8% decrease in frequencies gave the best fit to the experimental rate-energy data.

We have carried out calculations with these parameters as well. They are shown as the dashed lines in

Fig. 2. As can be seen they do not fit our results at all. The breakdown curves (calculated with our apparatus function) lie at too low an energy. Also, the sensitivity plot of crossover energy vs crossover shift shows that the discrepancy can not be removed by a small change in parameters (see Fig. 5, circle). It is clear that part of the difficulty lies in their choice of activation energy, 2.8 eV, which was based in part on the above mentioned electron impact experiment.⁶ This would lead to an underestimate of the activation energy.

There is more serious disagreement between the rate-energy dependence deduced by them and the one deduced in the present study. We calculated a rate energy curve using their parameters and in Fig. 7 compared the results to a set of values taken from their best-fit curve.³³ Our curve fits their values, indicating that this is not due to the difference in computational procedure (Laplace transform²³⁻²⁵ vs symmetric function theory^{34,35}). In Fig. 7 is also shown the rate energy curve deduced here; it differs from theirs by nearly an order of magnitude. Part of this is due to their apparent neglect of thermal rotational and vibrational energy. A crude estimate indicates that this produces an overestimate of at least a factor of 2 in the true rate. The rest remains unexplained. It would be interesting to see how well our present rate-energy results properly combined with the necessary thermal distributions, would reproduce the actual time of flight distribution measured by Baer *et al.*²⁰

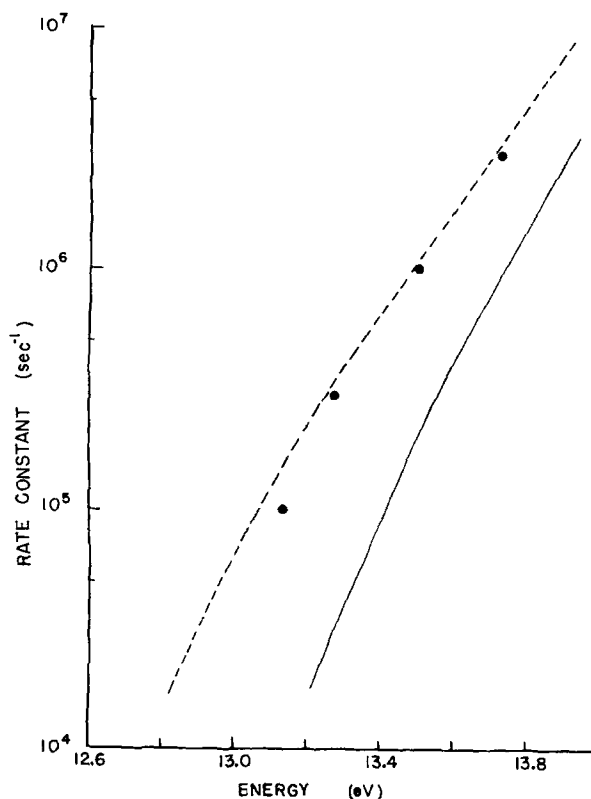


FIG. 7. Rate energy curves. (—) present calculations with activated complex parameters which reproduce the data in Fig. 2. (---) present calculations with activated complex parameters used by Baer *et al.*²⁰ (●) calculated by Baer *et al.*²⁰

The careful electron impact appearance potential analysis carried out by Bouchoux²¹ led to an estimated activation energy of 3.09–3.19 eV, in somewhat better agreement with our results.

D. Comparison with thermal reactions

The activation energy for the chlorobenzene ion fragmentation, 3.40 ± 0.05 eV, is equivalent to a 0 K bond energy. This can be compared to the corresponding bond energy of the neutral which can be calculated from the thermochemistry given earlier. The result is 4.2 eV. Thus the bond in the ion is ~ 0.8 eV weaker. If we imagine a hypothetical thermal decomposition of the chlorobenzene ion at 1000 K we can calculate an Arrhenius *A* factor from the activated complex properties. Depending on the model the results range from 6.6×10^{14} to 1.9×10^{15} . This may be compared to the preferred value of about 4×10^{15} for the thermal decomposition of bromobenzene at about 1000 K,³⁶ which should be similar in magnitude.

VI. CONCLUSIONS

The fragmentation of chlorobenzene ion in the 0.7–8.9 μ s time range is accompanied by a large kinetic shift (0.4 eV for these times measured at the crossover point). A systematic analysis of the time dependent breakdown curves can be carried out leading to an activation energy of 3.40 ± 0.05 eV and an equivalent 1000 K entropy of activation of 9.95 ± 0.4 eu. The activation entropy is indicative of a loose activated complex, and is similar in magnitude to the analogous thermal decomposition of bromobenzene at about 1000 K. The results lead to $\Delta H_{f_0}^\circ(\text{C}_6\text{H}_5^+) = 275 \pm 1$ kcal/mol and $\Delta H_{f_{298}}^\circ(\text{C}_6\text{H}_5^+) = 279 \pm 1$ kcal/mole. The systematic analysis of the data reveals energy–entropy compensation effects and clarifies the limits within which kinetic parameters and activated complex parameters can be established. Further, it is shown that the experiment and analysis lead to a quite accurate determination of the rate–energy curve in the range of 10^4 – 10^6 s⁻¹.

¹L. Friedman, F. A. Long, and M. Wolfsberg, *J. Chem. Phys.* **26**, 714 (1957).

²W. A. Chupka, *J. Chem. Phys.* **30**, 191 (1959).

³M. L. Gross, *Org. Mass Spectrom.* **6**, 327 (1972).

⁴R. A. W. Johnstone and F. A. Mellon, *J. Chem. Soc. Faraday Trans. II* **68**, 1209 (1972).

⁵P. Potzinger and G. von Büнау, *Ber. Bunsenges. Phys.*

Chem. **73**, 466 (1969).

⁶S. M. Gordon and N. W. Reid, *Int. J. Mass Spectrom. Ion Phys.* **18**, 379 (1975).

⁷C. Lifshitz, A. M. Peers, M. Weiss, and M. H. Weiss, *Adv. Mass Spectrom.* **6**, 871 (1974).

⁸C. Lifshitz, M. Weiss, and S. Landau–Gefen, Paper presented at the 25th Annual Conference on Mass Spectrometry, Washington, D. C., June 1977.

⁹H. M. Rosenstock, J. T. Larkins, and J. A. Walker, *Int. J. Mass Spectrom. Ion Phys.* **11**, 309 (1973).

¹⁰R. Stockbauer and H. M. Rosenstock, *Int. J. Mass Spectrom. Ion Phys.* **27**, 185 (1978).

¹¹C. J. Danby and J. H. D. Eland, *Int. J. Mass Spectrom. Ion Phys.* **8**, 153 (1972).

¹²R. Stockbauer, *J. Chem. Phys.* **58**, 3800 (1973); R. Stockbauer and M. G. Inghram, *ibid.* **62**, 4862 (1975).

¹³A. S. Werner and T. Baer, *J. Chem. Phys.* **62**, 2900 (1975).

¹⁴C. F. Batten, J. A. Taylor, and G. G. Meisels, *J. Chem. Phys.* **65**, 3316 (1976).

¹⁵J. Dannacher and J. Vogt, *Helv. Chim. Acta* **61**, 361 (1978).

¹⁶B. Andlauer and Chr. Ottinger, *J. Chem. Phys.* **55**, 1471 (1971).

¹⁷B. Andlauer and Chr. Ottinger, *Z. Naturforsch. Teil A* **27**, 293 (1972).

¹⁸W. A. Chupka, *J. Chem. Phys.* **54**, 1936 (1971).

¹⁹P. M. Guyon and J. Berkowitz, *J. Chem. Phys.* **54**, 1814 (1971).

²⁰T. Baer, B. P. Tsai, D. Smith, and P. T. Murray, *J. Chem. Phys.* **64**, 2460 (1976).

²¹G. Bouchoux, *Org. Mass Spectrom.* **12**, 681 (1977).

²²R. Stockbauer, *Int. J. Mass Spectrom. Ion Phys.* **25**, 89 (1977).

²³P. C. Haarhoff, *Mol. Phys.* **6**, 337 (1963).

²⁴H. M. Rosenstock, *Advan. Mass Spectrom.* **4**, 523 (1968).

²⁵W. Forst, *Chem. Rev.* **71**, 339 (1971).

²⁶D. H. Whitten, *J. Chem. Soc.* **1350** (1956).

²⁷A. S. Rodgers, D. M. Golden, and S. W. Benson, *J. Am. Chem. Soc.* **89**, 4578 (1967).

²⁸Yu. L. Sergeev, M. E. Akopyan, and G. I. Vilesov, *Opt. Spektrosk.* **32**, 230 (1972).

²⁹J. B. Pedley and J. Rylance, *Sussex–N. P. L. Computer Analysed Thermochemical Data: Organic and Organometallic Compounds*, University of Sussex (1977).

³⁰D. D. Wagman *et al.* Selected Values of Chemical Thermodynamic Properties, *Natl. Bur. Stand. Tech. Note 270–3* (U. S. Government Printing Office, Washington, D. C., 1968).

³¹W. Forst, *J. Phys. Chem.* **83**, 100 (1979).

³²J. L. Beauchamp, *Adv. Mass Spectrom.* **6**, 717 (1974).

³³Reference 20, Fig. 3.

³⁴M. L. Vestal, A. L. Wahrhaftig, and W. H. Johnston, *J. Chem. Phys.* **37**, 1276 (1962).

³⁵S. E. Buttrill, Jr., *J. Chem. Phys.* **52**, 6174 (1970).

³⁶S. W. Benson and H. E. O'Neal, "Kinetic Data on Gas Phase Unimolecular Reactions," *Natl. Bur. Stand. Ref. Data Ser. Natl. Bur. Stand.* **21** (February, 1970).